Supporting Information

Integrated Photoelectrochemical Energy Storage Cells Prepared by Benchtop Ion Soft-Landing

Venkateshkumar Prabhakaran[1,*], Joello Romo[1], Ashish Bhattarai[1], Kyle George[1], Zachary M. Norberg[1], David Kalb[1], Edoardo Aprà[2], Peter A. Kottke[3], Andrei G. Fedorov[3], Patrick Z. El-Khoury[1], Grant E. Johnson[1], Julia Laskin[4,*]

[1]Physical Sciences Division and [2]Environmental Molecular Sciences Laboratory, Pacific Northwest National Laboratory, Richland, WA 99352, USA.

[3]George W. Woodruff School of Mechanical Engineering, Georgia Institute of Technology, 771 Ferst Drive, Atlanta, GA 30332, USA.

[4]Department of Chemistry, Purdue University, West Lafayette, IN 47907, USA.

[*]Corresponding authors: venky@pnnl.gov; Grant.Johnson@pnnl.gov, Jlaskin@purdue.edu

Experimental

Chemicals

1-Ethyl-3-methylimidazolium tetrafluoroborate (EMIMBF$_4$) (99%), poly(vinylidene fluoride-*co*-hexafluoropropylene) (PVDF-HFP) (ACS grade), anhydrous N,N-dimethylformamide (DMF) (99.8%), sodium phosphotungstate hydrate (Na$_3$[PW$_{12}$O$_{40}$]xH$_2$O (98%), and ferrocenemethanol (98%) were all purchased from Sigma-Aldrich and used as received.

Preparation of Ionic Liquid-Ferrocenemethanol Membrane

A 2 g quantity of PVDF-HFP was dissolved in 13 mL of DMF. Next, 2 mL of EMIMBF$_4$ ionic liquid (IL) was added to the solution. To prepare IL membranes containing the ferrocenemethanol redox couple, 2 mL of a 10 mM ferrocenemethanol solution in DMF was added to the PVDF-HFP/EMIMBF$_4$ solution. The solution was stirred continuously for approximately 2 hours. The solution was cast in a glass petri dish and vacuum dried in an oven at 70°C for 10 hours. The thickness of the membrane was around ~100 µm.

Preparation of Photocathodes

The two types of WPOM photocathodes used in this study were prepared by (i) drop casting a salt solution of Keggin WPOM (Na$_3$PW$_{12}$O$_{40}$) in methanol directly onto the conductive side of indium-tin oxide (ITO) coated glass slides (10 x 10 mm) obtained from MTI Corporation and (ii) benchtop SL wherein only WPOM anions were deposited onto ITO.

The benchtop ion SL apparatus used in this work has been described in detail elsewhere.[1] Briefly, the dry ion localization and locomotion (DRILL) interface developed by Fedorov and co-workers[2] was modified to include a total of four electrospray emitters. A regulated pressure of heated N$_2$ gas (160°C) was used to desolvate the charged droplets produced by the electrospray emitters. An electrostatic pusher plate was used to direct only WPOM anions onto the electrode surface without counter cations and neutral solvent molecules, thereby achieving a uniform distribution of WPOM anions on the ITO surface. The deposition ion current of WPOM was measured using a picoammeter (model 9103, RBD Instruments, Bend, OR). Approximately equivalent numbers of ions (~10^{15} ions) were deposited onto the cathodes with each of the deposition methods.

Fabrication of Integrated Photoelectrochemical Energy Storage Cells

The IPES cells were fabricated by sandwiching together the WPOM photocathodes, IL-ferrocenemethanol membrane, and redox anode. Filter paper (Whatman, pore size: 70 µm, thickness: 200 µm, Grade 5 cellulose, catalog no.: 1005070) soaked in $EMIMBF_4$ was placed between the photocathode and ionic liquid membrane, which improved the separation between the redox couple and photocathode electrode surfaces (see Figure 1). We examined the performance of different substrates selected based on surface morphology as anodes. These included glassy carbon (GC), gold-coated silicon wafer (Au), ITO, and carbon nanotube coated (CNT) paper. The electro- and photo-chemical performance of the cell was optimized by changing the amount of POM deposited on the photocathodes, the concentration of ferrocenemethanol in the ionic liquid membrane, and the material used for the anode counter electrode.

Testing of Photoelectrochemical Cells

The IPES cells were irradiated with a 125 W/m^2 UV-Vis light source (Newport UV lamp) simulating the solar spectrum equipped with an attenuator, two collimators, and a fiber optic cable. Throughout these tests an auto-ranging picoammeter was used to measure the current and a Fluke 79 Series II multimeter was used to measure the voltage across the cell.

Intrinsic Electrochemistry of WPOM and Ferrocenemethanol

Cyclic voltammetry (CV) measurements of dropcast WPOM and ferrocenemethanol were performed to confirm their intrinsic redox activity on ITO and GC. A three electrode setup was employed in which the dropcast electrode was used as the working electrode, platinum wire as the counter electrode, and silver wire as the reference electrode. Pristine $EMIMBF_4$ was used as the electrolyte.

Hyperspectral Optical Absorption Microscopy

The macroscopic uniformity and aggregate formation of benchtop SL and drop cast WPOM on ITO photocathodes were characterized using hyperspectral optical microscopy. Approximately ~10^{15} WPOM ions were deposited using drop casting and benchtop SL and characterized as prepared by optical microscopy. The setup, data acquisition, and data analysis schemes are detailed elsewhere.[3, 4] For the current work, a custom illuminator based on a reflective collimator (Thorlabs,

Inc.) delivered incoherent white light (EQ-1500 LDLS, Energetiq Technology Inc.) to the samples. The samples were mounted onto the stage of an upright optical microscope (Zeiss Axio Imager 2M) equipped with a commercially available hyperspectral imager (Surface Optics, SOC710-VP, Spectral resolution: 4.7 nm). Image cubes were time-integrated for 20 ms and normalized to map spatially-resolved hyperspectral optical absorption with a pixel-limited spatial resolution of 435 nm.[3] The corresponding line profiles of optical absorption spectrographs were used to demonstrate the WPOM distribution and uniformity of films formed by drop casting and benchtop SL WPOM on ITO photocathode. Prior to characterization with hyperspectral optical microscopy, as-prepared drop cast and benchtop SL WPOM samples were imaged using a conventional Nikon Eclipse LV150N Digital Imaging system using 5x and 20x objectives to examine the macroscopic features at two different magnifications.

Raman Spectroscopy

The chemical state of drop cast and benchtop SL WPOM on ITO photocathodes was characterized using Raman micro-spectroscopy. The apparatus used for these measurements has been described in detail elsewhere.[5, 6] For this work, the top optical access was used to deliver 532 nm laser-irradiation through a 100X microscope objective (Mitutoyo, NA = 0.7). The back-scattered radiation was collected through the same objective, filtered through a dichroic beamsplitter/long pass filter assembly, and fiber-coupled to a spectrometer-CCD detection system (Andor, Shamrock 303i and iDus 416).

Approximately $\sim 10^{15}$ ions were deposited onto the ITO surface using drop casting and benchtop SL and the influence of counter cations on the electronic states of WPOM was assessed using Raman micro-spectroscopy. The data shown is spatially (100 spectra in a 10 x10 μm^2 area) and temporally (integration time of 1 sec) averaged to ensure sample integrity throughout the measurements. Simulations of the Raman spectra of WPOM were performed using a local version of NWChem.[7] The minimum energy structure of $PW_{12}O_{40}^{3-}$ was calculated using the B3LYP exchange-correlation functional in conjunction with the def2-TZVP basis set.[8] Molecular polarizability derivative tensors were computed at the same level of theory and the simulated spectrum was represented as a sum of Lorentzians centered at the predicted normal mode frequencies and broadened by 15 cm^{-1}. A single scaling factor of 0.976 was used to align the computed spectra to their experimental analogues.

In situ UV-Vis Spectroscopy

The photochromic transition of drop casted WPOM on ITO from clear to dark color was demonstrated by monitoring the changes in absorbance at visible wavelengths using *ex situ* and *in situ* UV-Vis spectroscopy during device operation. A Stellar Net Inc. Black Comet CXR-100 spectrometer coupled with a Stellar Net Inc. R600-8-VIS-NIR two-way fiber optic probe was used both to deliver UV-Vis light to the surface and to collect the reflected radiation. Absorbance spectra of the surface were recorded at different time intervals upon irradiation.

Electrochemistry of Photocathode and Redox Anode

Initially, the intrinsic electrochemical redox activity of WPOM and ferrocenemethanol in EMIMBF$_4$ ionic liquid was examined by CV on an ITO photocathode with a glassy carbon (GC) anode (Figure 1). The EMIMBF$_4$ ionic liquid was used as an electrolyte as it provides an enhanced potential window for WPOM. As expected, the CV of WPOM revealed multiple redox peaks, whereas that of Ferrocene showed only a single peak. The first reduction potential of WPOM was observed at 20 mV, whereas the oxidation potential of the Ferrocenemethanol redox couple was found at 220 mV. These results indicate that a potential difference of ~200 mV may develop across the IPES cell upon charging if WPOM undergoes photoredox reactions under irradiation. A higher potential (> 200 mV) may develop across the cell if WPOM goes to the second or third redox steps in the reduction process during irradiation as it absorbs more photons.
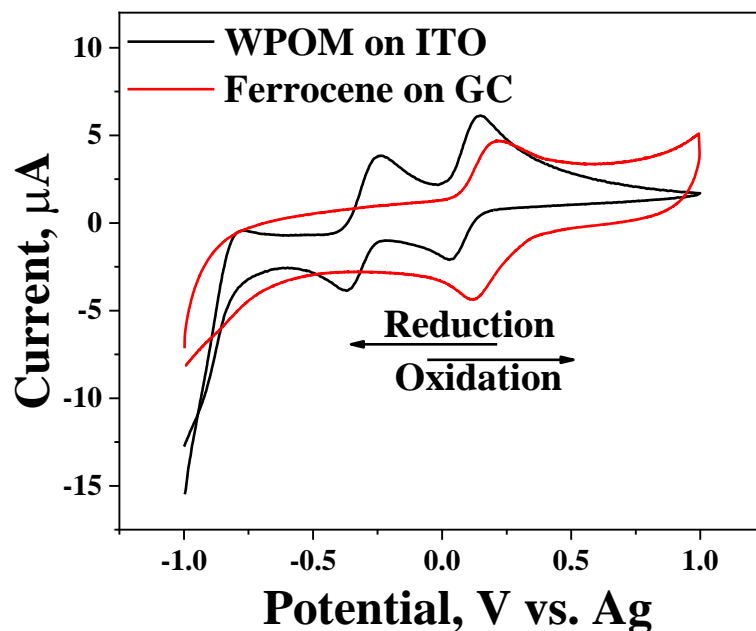
Figure S1. Representative cyclic voltammograms of solution drop cast WPOM and ferrocenemethanol on ITO and GC electrodes, respectively. Scan rate: 50 mVs^{-1}.

Effect of Surface Properties on the Counter Redox Reaction

The IPES cells were fabricated using EMIMBF$_4$ membranes, as described in the experimental section, and the effect of the surface properties of four different counter anodes such as GC, Au, ITO, and CNT on the kinetics of the ferrocenemethanol redox reaction were explored. The redox activity of ferrocenemethanol at the counter anode may act as a energy storage component of the IPES cell, and therefore influence the overall performance of the cell. These electrodes were chosen based on their surface morphology: planar (GC, Au, and ITO) and porous (CNT). Initially, the effect of using planar surfaces as redox anode on the performance of the IPES cells was evaluated using a WPOM drop cast photocathode.
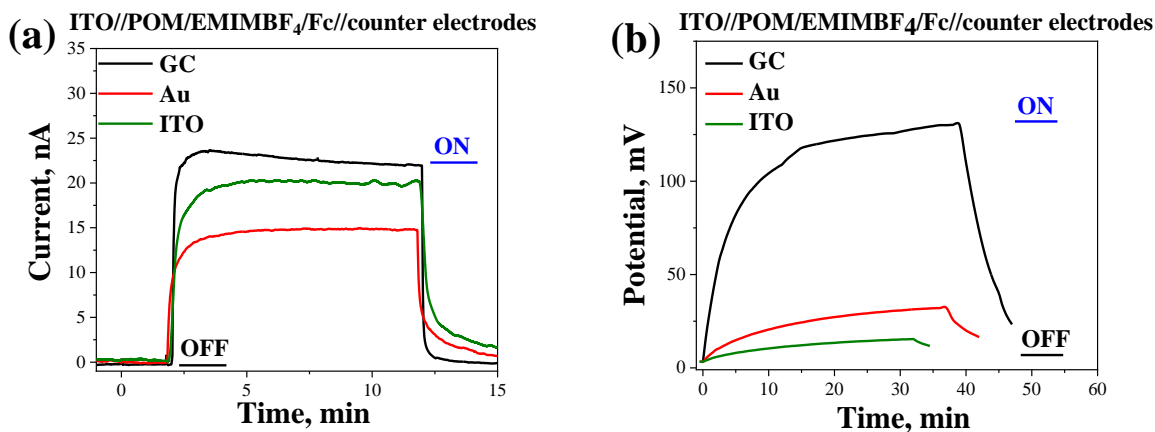
Figure S2. Representative charge-discharge profiles of IPES cells with planar surfaces such as GC, Au/Si, and ITO as counter anodes and WPOM dropcast photocathodes. (**a**) current response, (**b**) potential response. Approximately ~10^{15} WPOM ions were deposited using solution drop casting onto ITO photocathodes in each case.

The results obtained for planar electrodes are presented in Figure S2. The IPES cell with GC as the anode attained a maximum current of 25 nA and a potential of 125 mV. In contrast, we observed a maximum current of 20 nA and a potential of 15 mV for the cell containing the Au anode. A maximum current of 14 nA and a potential of 25 mV was observed for the cell containing an ITO anode. It is clear from these values that the IPES cell prepared using the GC anode shows a substantially larger photocurrent and potential across the cell in comparison with similar cells containing Au or ITO anodes. These observations are consistent with previous reports in the literature that showed the redox activity of ferrocenemethanol to be higher on GC compared to Au and ITO.[9-11] The IPES cell with GC as the anode also showed stable performance for three cycles tested as shown in Figure S3. Interestingly, the current response of IPES prepared with benchtop SL WPOM showed improvement over cycles. This observation may be attributed to formation of a more stable performing interface in the absence of strongly coordinating counter ions compared to the IPES prepared with drop cast WPOM.
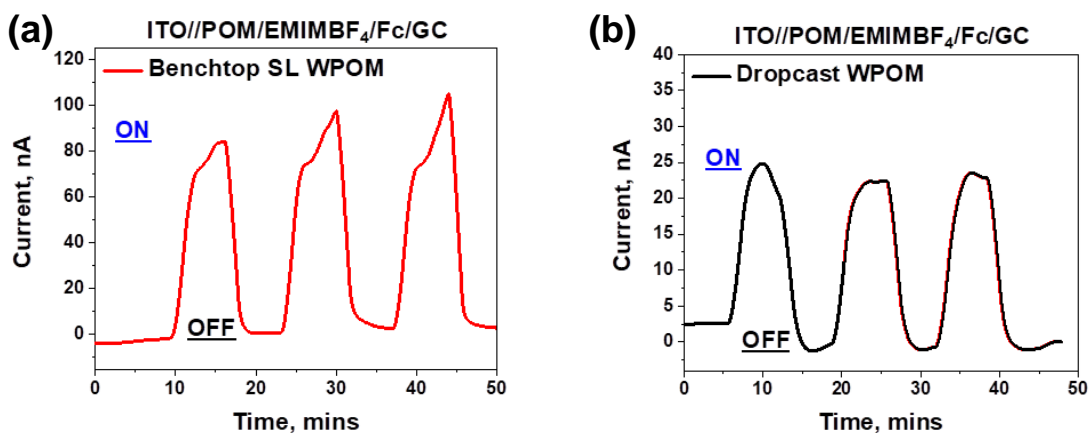
Figure S3. Photocharge-discharge current response profiles of IPES cells with drop cast and benchtop SL WPOM on ITO cathodes using GC as the counter anodes measured continuously for three cycles. Approximately ~10^{15} WPOM ions were deposited onto ITO in each experiment.

Following the observation of higher performance of GC as the anode, the intrinsic electrochemical redox activity of both WPOM and ferrocenemethanol on ITO and GC were determined to reaffirm the activity on their respective electrodes. Overall, this experiment established the working principle of the IPES cell which is derived from the redox activity of WPOM and ferrocenemethanol and confirms that the redox reaction of WPOM in an operating IPES cell is driven by photon absorption.

Photochromism of WPOM at Photocathodes

Using WPOM as both photon- and electron-trapping centers at the photochemical interface is a unique feature of the IPES demonstrated herein. The photochromic properties of WPOM are another unique property of the WPOM-based IPES cell compared to other types of photoelectrochemical cells reported in the literature. Photochromism in IPES is caused by the reduction of WPOM when exposed to irradiation. According to literature data, the most prominent process upon irradiation of WPOM is a four-electron photoreduction from the 3- to 7- charge state.[12] *Ex situ* UV-Vis absorbance spectroscopy experiments were performed to study the intrinsic photochromism of WPOM on ITO cathodes prepared by drop casting and benchtop SL. Photographic images of drop cast and benchtop SL WPOM on ITO cathodes before and

immediately after irradiation for 10 mins are shown in Figure S4 (a and c), respectively. The change of the ITO surface from clear to darkened blue in color in both cases confirms the reduction of WPOM on ITO. The corresponding absorption spectra measured on both ITO cathodes before and after irradiation are shown in Figure S4 (b and d), respectively. An increase in absorption is observed in the visible region (450 - 700 nm), which is in line with observation with the naked eye. Moving forward, the photochromism of WPOM upon reduction during IPES cell operation was explored by taking absorption measurements on the drop cast WPOM ITO side of the cell *in situ* as shown in Figure S4. During irradiation we observed a substantial increase in absorption at 490, 515, and 585 nm which corresponds to the blue, green, and yellow regions of the visible spectrum, respectively. The formation of new absorption peaks at multiple wavelengths in the visible region in the UV-Vis spectrum during irradiation is attributed to the transition of WPOM through multiple redox steps.

Additionally, *in situ* absorption measurements were performed on drop cast WPOM on ITO in the assembled IPES cell as a model system. A substantial increase in absorption due to the photochromic redox transition of WPOM on ITO was observed at 490, 515, and 585 nm corresponding to the blue, green, and yellow regions of the visible spectrum, respectively (see Figure S5). This result further corroborates the unique features of photochromic WPOM in the IPES which suggests additional possibilities (*e.g.,* smart windows) for the newly developed light harvesting and storage technology.
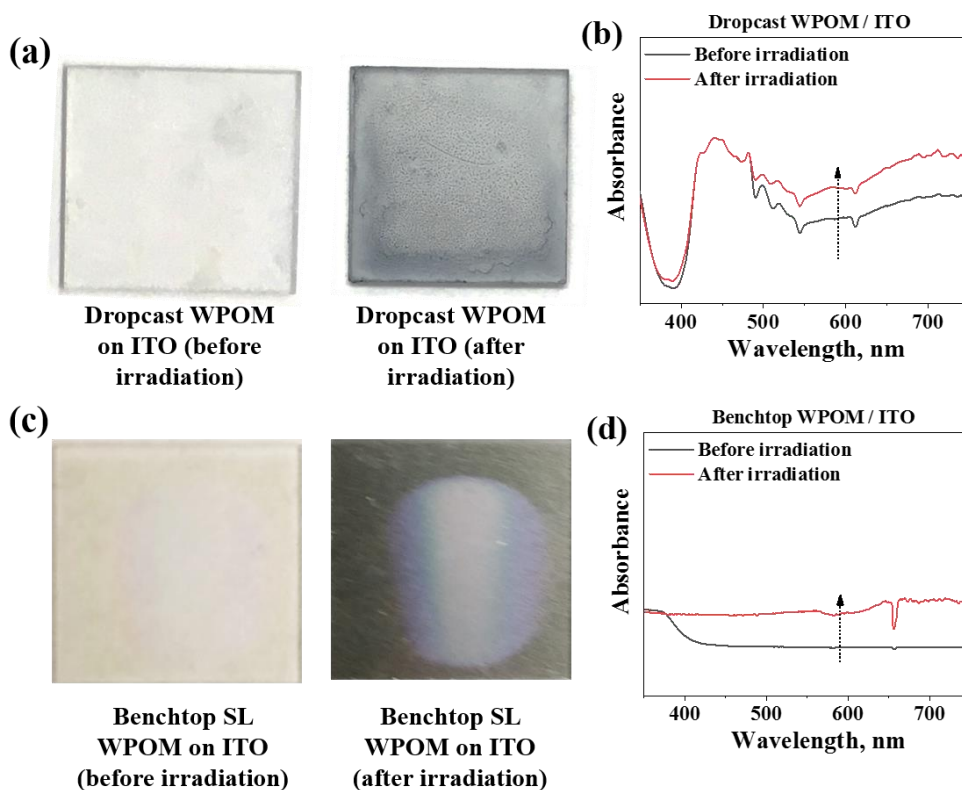
Figure S4. Photochromism of WPOM on ITO upon irradiation (a) photographic image of drop cast WPOM before and after irradiation, (b) corresponding *ex situ* UV-Vis absorption spectra of drop cast WPOM before and after irradiation, (c) photographic image of benchtop SL WPOM before and after irradiation, (d) corresponding *ex situ* UV-Vis absorption spectra of benchtop SL WPOM before and after irradiation. Approximately ~10^{15} WPOM ions were deposited onto ITO in each case.
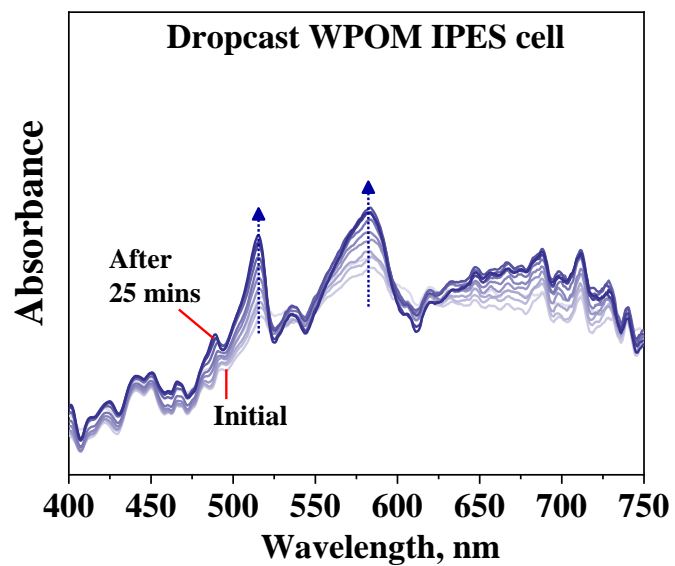
Figure S5. *In situ* UV-Vis absorption spectra measured on a working dropcast WPOM IPES cell demonstrating the photochromism induced by WPOM at different irradiation time intervals (0 to 25 mins).
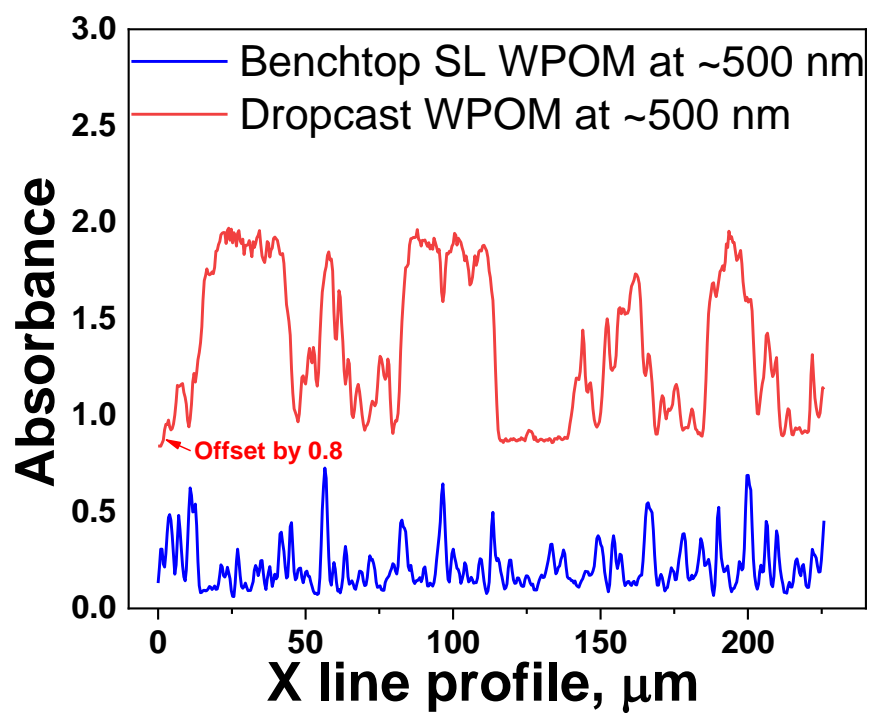
Figure S6. Spatially-resolved line profile obtained on benchtop SL and drop cast WPOM on ITO using hyperspectral optical bright field absorption spectroscopy at ~500 nm, showing the variations in the absorbance intensity across the 250 µm line.
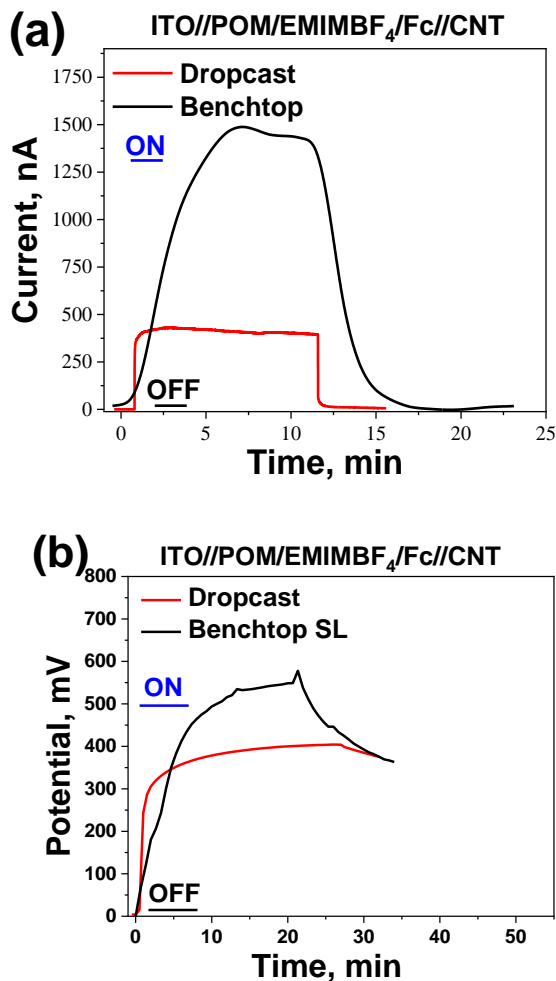
Figure S7. Charge-discharge profiles of IPES cells with CNT paper as the counter electrode. Effect on drop cast and benchtop SL photocathode based cells are compared. (a) current response, (b) potential response. Approximately ~10^{15} WPOM ions were deposited onto ITO in each case.

References

1. G. E. Johnson, V. Prabhakaran, N. D. Browning, B. L. Mehdi, J. Laskin, P. A. Kottke and A. G. Fedorov, *Batter Supercaps*, 2018, **1**, 97-101.
2. P. A. Kottke, J. Y. Lee, A. P. Jonke, C. A. Seneviratne, E. S. Hecht, D. C. Muddiman, M. P. Torres and A. G. Fedorov, *Anal. Chem.*, 2017, **89**, 8981-8987.
3. I. V. Novikova, C. R. Smallwood, Y. Gong, D. Hu, L. Hendricks, J. E. Evans, A. Bhattarai, W. P. Hess and P. Z. El-Khoury, *Chem. Phys.*, 2017, **498-499**, 25-32.
4. P. Z. El-Khoury, A. G. Joly and W. P. Hess, *J Phys Chem C*, 2016, **120**, 7295-7298.
5. A. Bhattarai, A. G. Joly, W. P. Hess and P. Z. El-Khoury, *Nano Lett.*, 2017, **17**, 7131-7137.
6. A. Bhattarai and P. Z. El-Khoury, *Chem Commun (Camb)*, 2017, **53**, 7310-7313.
7. M. Valiev, E. J. Bylaska, N. Govind, K. Kowalski, T. P. Straatsma, H. J. J. Van Dam, D. Wang, J. Nieplocha, E. Apra, T. L. Windus and W. de Jong, *Comput. Phys. Commun.*, 2010, **181**, 1477-1489.
8. F. Weigend and R. Ahlrichs, *Phys. Chem. Chem. Phys.*, 2005, **7**, 3297-3305.

9.   M. H. Pournaghi-Azar and R. Ojani, *Electrochim. Acta*, 1994, **39**, 953-955.
10.   N. Frenzel, J. Hartley and G. Frisch, *Phys. Chem. Chem. Phys.*, 2017, **19**, 28841-28852.
11.   S. Bouden, A. Dahi, F. Hauquier, H. Randriamahazaka and J. Ghilane, *Sci Rep*, 2016, **6**, 36708.
12.   T. Yamase, *Chem. Rev.*, 1998, **98**, 307-326.